(1)

Quarterly Technical Report

Growth, Characterization and Device Development in Monocrystalline Diamond Films

Supported under Grant #N00014-93-I-0437
Office of the Chief of Naval Research
Report for the period 4/1/94–6/30/94

R. F. Davis, J. T. Glass, and R. J. Nemanich*
K. S. Ailey, J. Avent, D. J. Kester, and B. R. Stoner
North Carolina State University
c/o Materials Science and Engineering Department
*Department of Physics
Raleigh, NC 27695

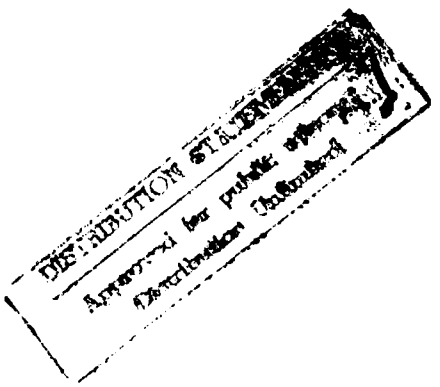

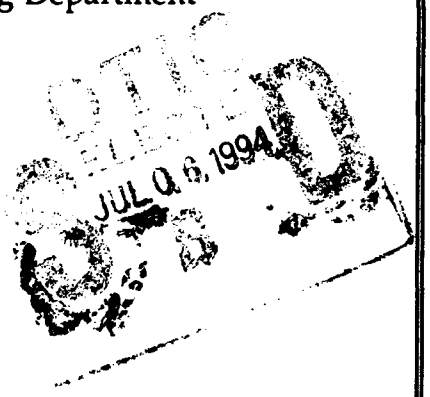

June, 1994

34pg

REPORT DOCUMENTATION PAGE

Form Approved
OMB No. 0704-0188

1. AGENCY USE ONLY *(Leave blank)*	2. REPORT DATE	3. REPORT TYPE AND DATES COVERED
	June, 1994	Quarterly Technical 4/1/94–6/30/94

4. TITLE AND SUBTITLE
Growth, Characterization and Device Development in Monocrystalline Diamond Films

5. FUNDING NUMBERS
s400003srr14
1114SS
N00179
N66005
4B855

6. AUTHOR(S)
Robert F. Davis, J. T. Glass and R. J. Nemanich

7. PERFORMING ORGANIZATION NAME(S) AND ADDRESS(ES)
North Carolina State University
Hillsborough Street
Raleigh, NC 27695

8. PERFORMING ORGANIZATION REPORT NUMBER
N00014-93-I-0437

9. SPONSORING/MONITORING AGENCY NAMES(S) AND ADDRESS(ES)
Sponsoring: ONR, Code 1114, 800 N. Quincy, Arlington, VA 22217-5660
Monitoring: Office of Naval Research Resider
The Ohio State University Research Center
1960 Kenny Road
Columbus, OH 43210-1063

10. SPONSORING/MONITORING AGENCY REPORT NUMBER

11. SUPPLEMENTARY NOTES

12a. DISTRIBUTION/AVAILABILITY STATEMENT
Approved for Public Release; Distribution Unlimited

12b. DISTRIBUTION CODE

13. ABSTRACT *(Maximum 200 words)*

Diamond hot wire anemometers were fabricated and tested in a hybrid constant current, constant temperature mode. Wires were tested for response time, sensitivity and reproducibility, with the objective being to observe the effects of geometrical variations on these properties. Results indicated no strong correlation between geometry and response time. Sensitivity measurements also showed little difference among geometries. Research continued in the growth of boron nitride films on various substrates including Si(100), diamond (100), Cu (100) and Ni(100) via ion beam assisted electron beam evaporation. Fourier transform infrared spectroscopy and high resolution transmission electron microscopy showed that the total films on Si and diamond consisted of the sequence from the substrate: a-BN, h-BN, c-BN. The c-BN layers formed as a function of deposition temperature, ion current and thickness. The occurrence of this layer is attributed to increasing intrinsic biaxial compressive stress generated during deposition.

14. SUBJECT TERMS
diamond, hot wire anemometers, geometry, response time, boron nitride films, a-BN, h-BN, c-BN, Si, Cu, Ni, diamond, biaxial compressive stress

15. NUMBER OF PAGES
31

16. PRICE CODE

17. SECURITY CLASSIFICATION OF REPORT	18. SECURITY CLASSIFICATION OF THIS PAGE	19. SECURITY CLASSIFICATION OF ABSTRACT	20. LIMITATION OF ABSTRACT
UNCLAS	UNCLAS	UNCLAS	SAR

Table of Contents

I. Introduction

Diamond as a semiconductor in high-frequency, high-power transistors has unique advantages and disadvantages. Two advantages of diamond over other semiconductors used for these devices are its high thermal conductivity and high electric-field breakdown. The high thermal conductivity allows for higher power dissipation over similar devices made in Si or GaAs, and the higher electric field breakdown makes possible the production of substantially higher power, higher frequency devices than can be made with other commonly used semiconductors.

In general, the use of bulk crystals severely limits the potential semiconductor applications of diamond. Among several problems typical for this approach are the difficulty of doping the bulk crystals, device integration problems, high cost and low area of such substrates. In principal, these problems can be alleviated via the availability of chemically vapor deposited (CVD) diamond films. Recent studies have shown that CVD diamond films have thermally activated conductivity with activation energies similar to crystalline diamonds with comparable doping levels. Acceptor doping via the gas phase is also possible during activated CVD growth by the addition of diborane to the primary gas stream.

The recently developed activated CVD methods have made feasible the growth of polycrystalline diamond thin films on many non-diamond substrates and the growth of single crystal thin films on diamond substrates. More specifically, single crystal epitaxial films have been grown on the {100} faces of natural and high pressure/high temperature synthetic crystals. Crystallographic perfection of these homoepitaxial films is comparable to that of natural diamond crystals. However, routes to the achievement of rapid nucleation on foreign substrates and heteroepitaxy on one or more of these substrates has proven more difficult to achieve. This area of study has been a principal focus of the research of this contract.

At present, the feasibility of diamond electronics has been demonstrated with several simple experimental devices, while the development of a true diamond-based semiconductor materials technology has several barriers which a host of investigators are struggling to surmount. It is in this latter regime of investigation that the research described in this report has and continues to address.

In this reporting period, diamond hot wire anemometers were fabricated and tested in a hybrid constant current, constant temperature mode. Wires were tested for response time, sensitivity and reproducibility, with the objective being to observe the effects of geometrical variations on these properties. Continued research was also conducted in the growth of boron nitride films on various substrates including Si(100), diamond (100), Cu (100) and Ni(100) via ion beam-assisted electron beam evaporation. Fourier transform infrared spectroscopy and high resolution transmission electron microscopy were employed for the characterization of the a-BN, h-BN and c-BN films which were deposited.

The following subsections detail the experimental procedures for each of the aforementioned studies, discuss the results and provide conclusions and references for these studies. Note that each major section is self-contained with its own figures, tables and references.

II. Geometrical Effects on the Flow Response of a Diamond Thin Film Hot Wire Anemometer

A. Introduction

Hot Wire Anemometry. Hot wire anemometers belong to a class of flowmeters that are based on the energy additive approach. For this technique, an outside source of energy is introduced to the flowing fluid, and the effect of the fluid on the energy source or the effect of the energy source on the fluid is monitored. For hot wire anemometers, the former condition prevails.[1] The thermo-element of this device is a fine wire which is usually connected as an arm of a Wheatstone bridge configuration. One can consider the amount of heat, q, given off from the sensor to the flow as:

$$q = 0.24I^2R \tag{1}$$

where I is the current, and R is the resistance in the film. In terms of fluid properties:

$$q = (t_s - t_g)\,[C_t + (2\pi dC_v\rho V)^{1/n}] \tag{2}$$

where t_s is the wire temperature, t_g = fluid temperature, C_t = thermal conductivity of the fluid, d = wire diameter, C_v = heat capacity of the fluid at constant volume, ρ = fluid density, V = fluid velocity, and n is approximately equal to 2. The equations show that hot wire anemometers are mass flow sensitive, by the term ρV, and dependent upon fluid composition due to the C_t and C_v terms.[1] The exponent, n, was determined by L.V. King, who studied the relationship between the power required to maintain a constant temperature at a given flow rate. This dependence was determined to be linear if the square root of the flow rate was plotted on the abscissa.[2]

These probes can fall into two operative categories, constant current or constant temperature. In a constant current anemometer, the rate of flow is measured as a variation in the element's resistance for a supplied current of constant magnitude; in a constant temperature anemometer, the flow rate is measured as a function of variation in magnitude of the current for an element whose resistance, or temperature, is held constant.[3] Thermo-anemometers are nonlinear in current or voltage output versus velocity, and a linearizing circuit is usually employed in the constant temperature configuration. Although constant current probes are easier to design, constant temperature anemometers offer many advantages, including higher signal to noise ratio, longer probe life, and circuitry compatibility with the wire's frequency characteristics.[1] Constant current devices suffer from a feature called burnout in which sudden or rapid cooling of the wire can destroy it.[3] For this work, the anemometers were hybrids of constant current and constant temperature anemometers. Constant current was supplied to the films via a heater coil to keep the heater side temperature of the structures constant.

Historical wire materials of hot wire anemometers include copper, tungsten, and platinum, and some alloys such as platinum-iridium and platinum-rhodium[3]. These sensors are utilized in many applications such as air conditioning and heating systems, wind tunnels, and mass flow controllers.

Advantages of Diamond. Diamond's high thermal diffusivity and chemical inertness make it a good material to use in flow sensor applications where a short response time and resistance to corrosive fluids are desired. Diamond can also be used at higher temperatures than other materials.[4] Its melting point is higher than that of its conventional semiconducting counterpart, silicon.

Diamond has been shown to exhibit a step-response of more than a factor of two faster than an all-silicon device of the same dimensions in the same hot wire anemometer configuration. However, in the devices tested, some silicon remained under the diamond because complete etching of the silicon would have caused the diamond films to rupture.[5] The potential of a free-standing diamond film has yet to be realized.

In this work, various wire geometries of free-standing diamond are tested for response and sensitivity. The purpose is to observe the effects of changes in length, width, and thickness on the response times and sensitivities of hot wire anemometer structures.

B. Experimental Procedure

Device Fabrication. Microwave plasma chemical vapor deposited (MPCVD) diamond films of thicknesses approximately 15 mm and 40 mm were grown on silicon substrates at Kobe Steel, Electronic Materials Center. Scanning electron micrographs were taken to measure the thicknesses and observe film topography. No significant differences were observed in the films of different thickness. A Spex Raman system (incident wavelength, $\lambda = 514.5$ nm and spot size = 4 μm) was used to show that the films were in fact diamond by the peak around 1332 cm^{-1}. The wafers were diced into the desired geometries, then etched in a 1:1:1 by volume solution of $HF\text{-}HNO_3\text{-}H_20$(deionized) to remove the diamond films completely from the silicon substrates. Next, the films were epoxied onto Macor supports which contained channels through which fluid could flow. A coil of NiCr wire around alumina epoxied to one end of the film functioned as a heater, and a thermocouple epoxied to the other end measured changes in temperature of the film due to cooling by the gas. A schematic of the device is depicted in Fig. 1.

Eight different geometries were chosen in which length, width, and thickness were varied. Using the relationship for internal thermal conductance[6],

$$K = \kappa(A/L), \tag{3}$$

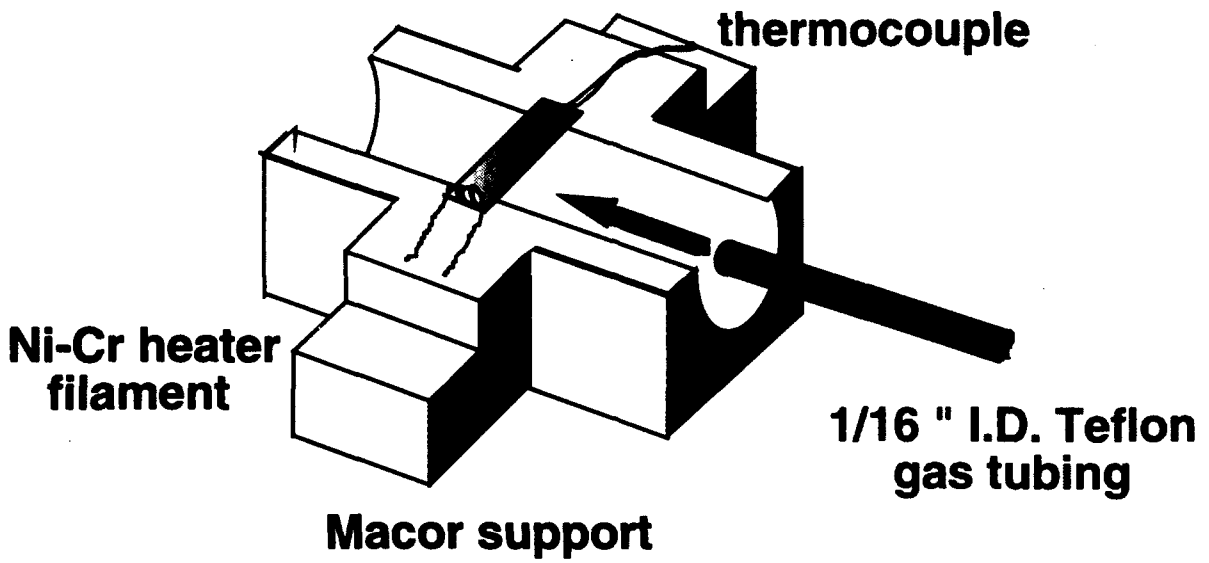

Figure 1. Schematic of the hot wire anemometer structure. The heater temperature remains constant at To, and the thermocouple temperature, T, changes with time.

where κ is the thermal conductivity, A is the cross-sectional area of the wire, and L is the wire length. It was speculated that a wire of larger cross-sectional area to length ratio should exhibit the greatest thermal conductance, therefore yielding the fastest response to changes in temperature. Further research, however, indicated that convective cooling rates were dependent upon surface area:volume, not thermal conductance.

Initial Testing. Figure 2 depicts the testing apparatus. A current limiting power source supplied constant current to the heating element of the wires. Temperature changes were sensed on the "cold" end by teflon insulated, 36-gauge, chromel/alumel thermocouples connected to an Omega multimeter. A rotameter-type flow meter was used to monitor and adjust the flow rates of the argon gas. The gas line, with an inside diameter of 0.0625", was placed inside the channel of the Macor support 28 mm from the edge of the film. It was held in place with Teflon tape across the channel edges. In this manner, it was assumed that the flow profiles from the gas line to the films would be similar for each geometry. Later, upon testing the flow characteristics as the velocity was increased from 1 to 4 l/min, it was observed that the gas was spreading significantly from the tube end to the film edge, causing direct cooling of the heater element. The second part of this paper describes a new testing apparatus designed to alleviate the problem of heater side cooling.

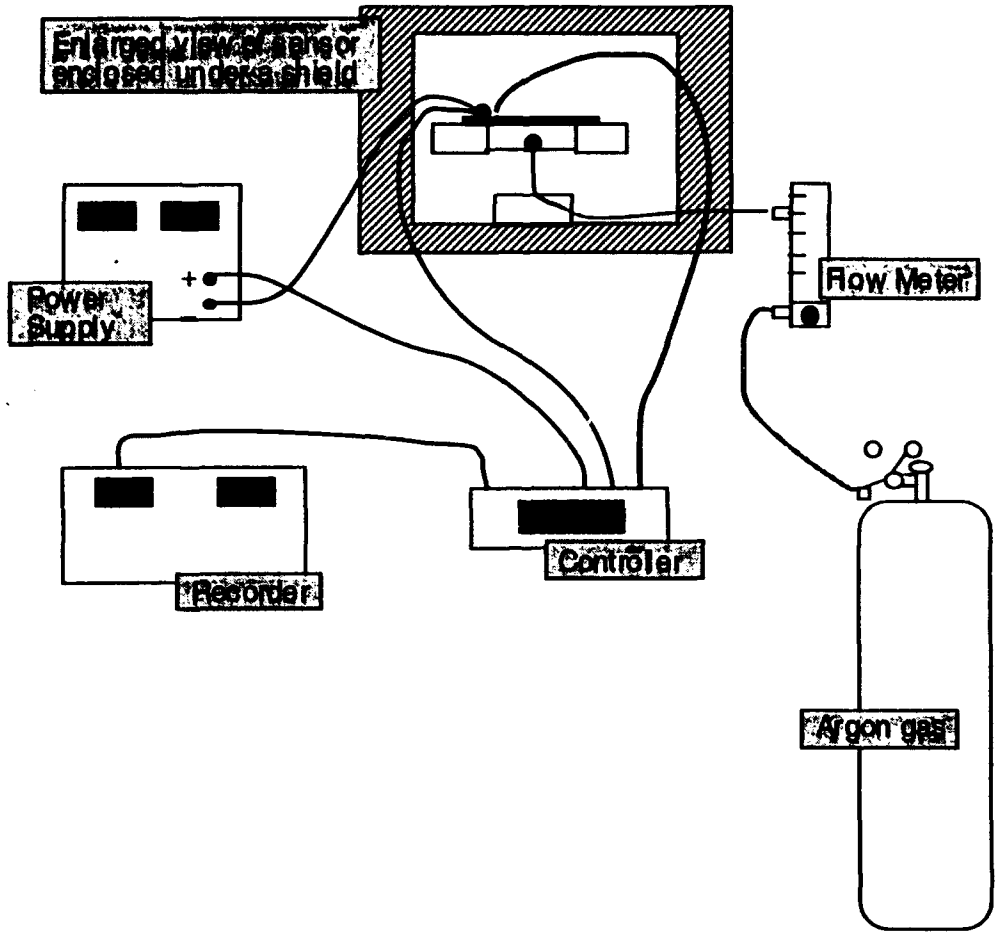

Figure 2. Schematic of the anemometer testing system. The temperature controller was not used in the initial characteristic measurements.

Several types of measurements were used to characterize the wires. King's law is a commonly accepted heat transfer calibration law for hot wire anemometers. It states that the power required to maintain a constant temperature varies linearly with the square root of the mass flow rate[3,5]. The calibration data for three geometries (10mm × 4mm × 15μm, 20mm × 1mm × 40μm, and 10mm × 4mm × 40μm) was used to test agreement of the diamond hot wire anemometer structures with King's law. For this measurement, an initial current was supplied to the wires, and the temperature was allowed to stabilize in the absence of flow. The flow was then turned on, and a temperature drop in the wires was observed. When the temperature stabilized again, the current was increased until the wire heated to the initial temperature. The flow rate was then increased, and the same procedure followed to the highest flow rate utilized. This raw calibration data was then applied to the form

$$P = A + B\,U^{0.5} \tag{4}$$

where P = input power, U = flow velocity, and A and B are empirically determined calibration constants.

For transient response measurements from zero flow at time t = 0, the change in temperature at the thermocouple end of the devices was monitored at ten-second intervals for 120 seconds while argon gas flowed perpendicular to the wires' axes at flow rates of 1, 2, 3, and 4 l/min. The devices were also measured under the influence of doubling the flow rate from 2 to 4 l/min. The response of anemometers to an increase in non-zero flow rates simulates real world situations in which one would like to know the flow rate of a fluid at time t. For these tests the wires were heated and the temperatures allowed to stabilize. Temperature changes were monitored at 10s intervals for 120s at 2 l/min; then the flow rate was immediately increased to 4 l/min to observe the response of doubling the flow rate in transient. Reproducibility measurements between changes in temperature for each run at each flow rate were recorded and reported in terms of standard deviation.

The sensitivity of the wires was extrapolated from transient response data to determine the devices' abilities to measure small variations in flow rate. The slope of curves of ΔT vs. the square root of the flow rate was taken as a sensitivity measurement.

C. Results and Discussion

The calibration data of power versus the square root of the velocity did not agree well with King's law (see Eq. 4). Curve fits were exponential instead of linear (see Fig. 3). However, there are other empirical calibration laws used in hot wire anemometry. Collis and

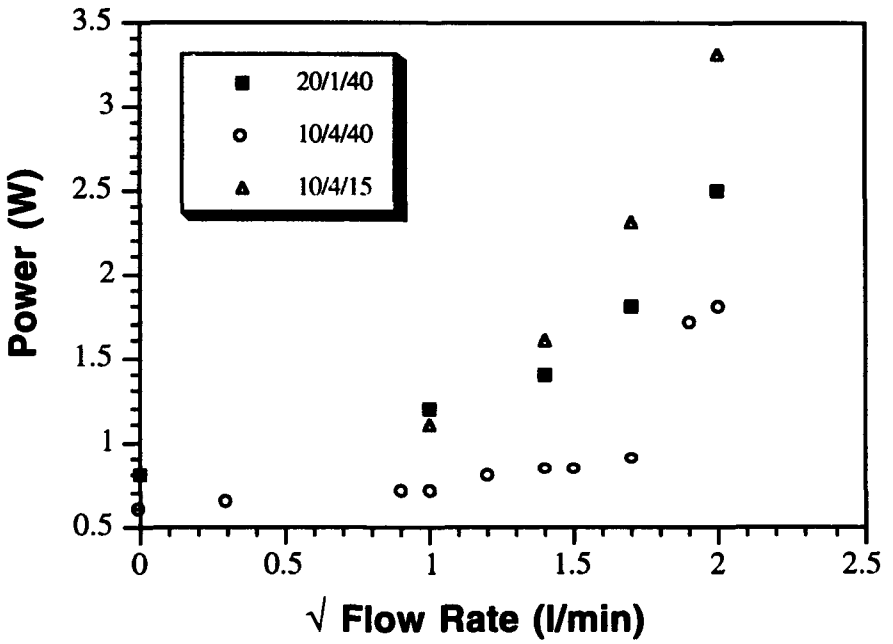

Figure 3. King's law curves for three geometries. The dashed line indicates the expected linear dependence of the power required to maintain a constant temperature at a given flow rate.

Williams obtained the best fit for their experimental data using a simple exponential power law with exponents equal to 0.43 and 0.45 [7,8]. By trial and error, the exponents for geometries 10mm × 4mm × 15μm and 20mm × 1mm × 40μm were determined to be 1.7 and 1.5, respectively. The exponent for the geometry 10mm × 4mm × 40μm is assumed to be $n \geq 2$, but due to the large deviation from empirical exponents found in the literature, it was not deemed necessary to make the fit converge.

Figure 4 shows the characteristic response for a solid object undergoing transient heating or cooling. The change in temperature vs. time is depicted for all eight geometries as the flow rate is increased from 0 to 3 l/min. Devices were characterized using a model for unsteady state conditions in one dimension in a solid, where the solid material has a high thermal conductivity so that the temperature within the solid can be considered essentially uniform at any time.[9] For the case at hand, a heated wire with an initial temperature T_o at time $t = 0$ is immersed into a cooler fluid at temperature T^* that is constant with time. It is assumed that the heat transfer coefficient is constant with time. The 90% response time is defined as 0.9θ, where θ is equivalent to the left side of Eq. 5. In other words it is the time required for the film to cool to 90% of its asymtotic value. In order to determine the 90% response times for each geometry, the following equation is utilized [9]:

$$(T - T^*)/(T_o - T^*) = e^{-(hA/c_p\rho V)t} \tag{5}$$

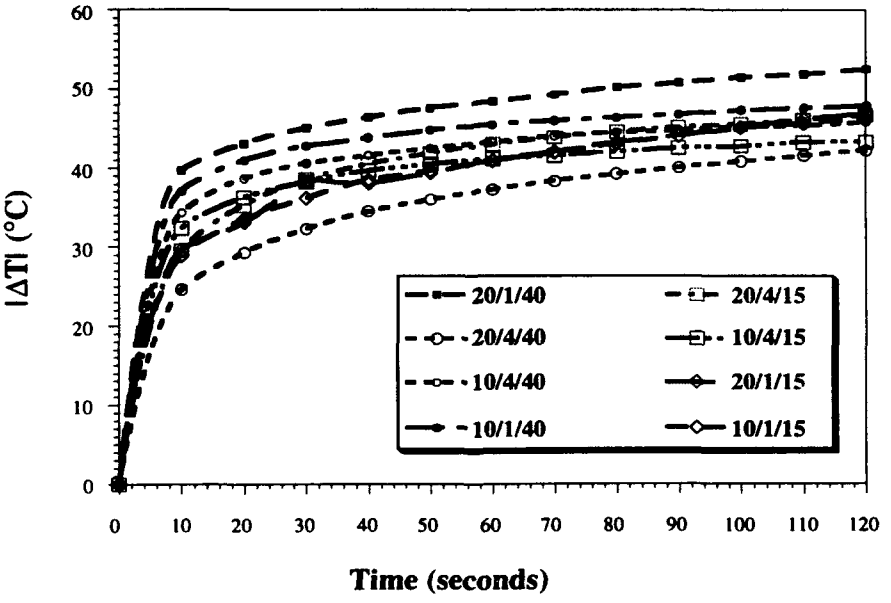

Figure 4. Response of all geometries to transient cooling as the flow rate is increased from 0-3 l/min. The numbers in the legend indicate the different lengths, widths and thicknesses tested.

which describes the time-temperature history of the wires. T is the temperature at time t, T* is the fluid temperature, T_o is the initial temperature of the wire at time t = 0, h is the heat transfer coefficient, A is the surface area of the wire, c_p is the constant pressure heat capacity, ρ is the wire density, V is the wire volume, and t is time. This equation indicates that the surface area:volume ratio of the object must be known.[9] As stated above, the assumption of negligible internal resistance (high thermal conductivity) was made. The assumption is valid when the Biot number, $Bi = hx_i/\kappa$, where x_i is a characteristic dimension of the body is less than 0.1. For a long rod $x = V/A = [(2x)^2L]/[4(2x)L]$ or half the thickness of the rod.[9]

Figure 5 shows the response time versus surface area:volume. No strong correlation existed between geometry and response time. It was expected that as surface area:volume increased the response time would be faster, following the relationship indicated by the dashed line on Figure 5. Reproducibility measurements of the change in temperature were very good, however, indicating that systematic errors were minimal. Average standard deviations of the four flow rates ranged from 0.4 to 1σ, with the lowest error occurring in the sample with surface area:volume 1333 cm^{-1} (10mm × 1mm × 15μm), and the highest error occurring in the sample with surface area:volume 625 cm^{-1} (20mm × 4mm × 40μm).

Sensitivity curves of ΔT vs. the square root of the flow rate are shown in Fig. 6 for all eight wires, and the slope of the curves are used as an indication of sensitivity. The slopes for

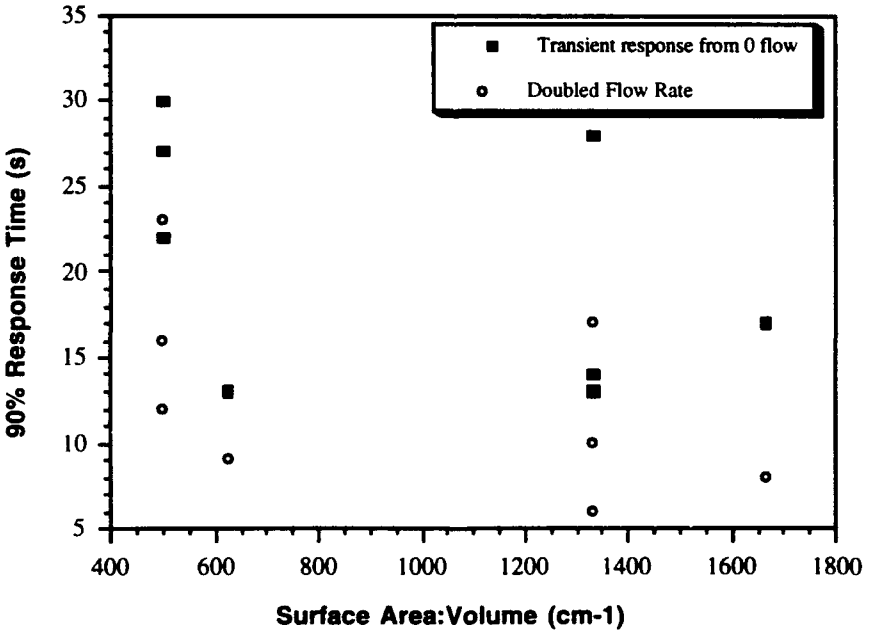

Figure 5. This graph shows the geometrical effects on response time. The 90% response time is plotted for each geometry (at their respective surface area:volume) for flow rates of 0 to 3 l/min and 2 to 4 l/min. The dashed line indicates a theoretical dependence of response time on surface area:volume based on Eq. 5.

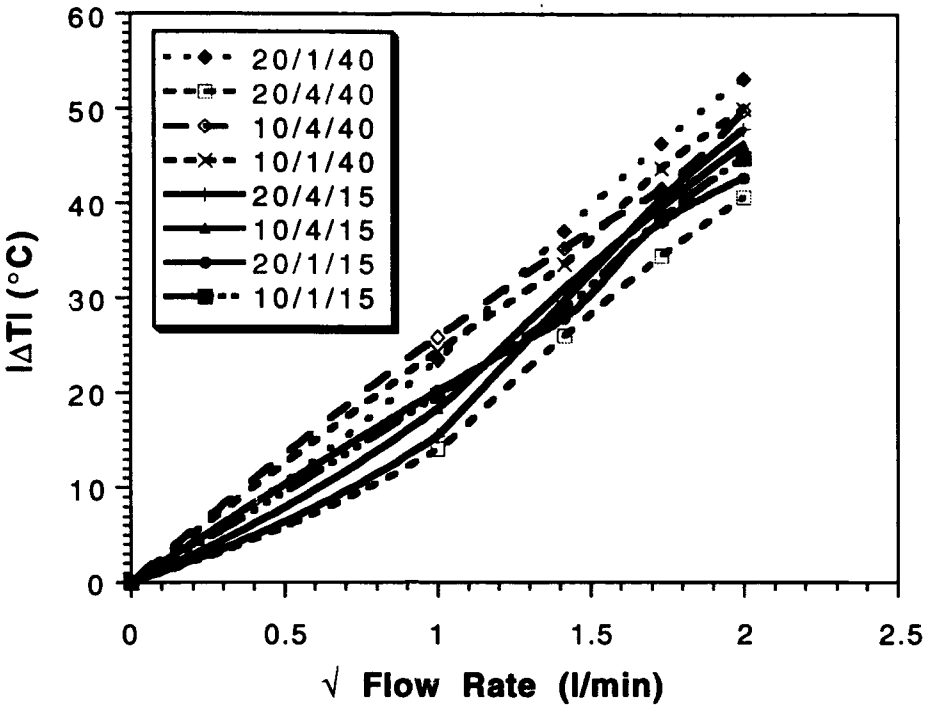

Figure 6. Sensitivity curves for each geometry. Slope values were used as an indication of sensitivity.

each geometry are very close, contrary to the expectation that a large difference in surface area:volume should produce more variation in sensitivity. According to an equation for heat flux due to convection[10],

$$Q = h\Delta TF\tau \tag{6}$$

where Q = the quantity of heat given off or taken up by the fluid, h = the heat transfer coefficient, DT = the difference between the average temperatures of the film surface and the fluid, F = the surface area of the solid in contact with the fluid, and t = time, as the surface area:volume increases the sensitivity should increase.

Analysis of Testing Apparatus. Due to the closeness of slope values, it was speculated that the experimental apparatus was not accurate enough for this calibration process. It was observed that the gas was spreading significantly from the tube end to the film edge, thus cooling the heater element. At 1 l/min the flow pattern was laminar; as the flow rate was increased more eddies due to turbulence were apparent, and dispersion of the gas was observed. Reasons for the gas spread may have included lack of isolation of the heater element from the gas, employment of gas tubing with a very small inside diameter, and improper placement of the tubing.

To test the experimental procedure, a new system was designed using a temperature controller to maintain the hot side of the wires at ~180°C, and a gas line with an inside

diameter of 0.12" was placed 3.5mm from the film to try to eliminate spread of the gas to the heater. The flow rates used were 1, 1.5, 2, 2.2, and 3 l/min. Samples 3 and 7, which exhibited a large variation in surface area:volume, were tested for sensitivity, and the results are shown in Fig. 7. The data from the measurements made with the new testing apparatus is plotted on the same axes as the original sensitivity curves. A large temperature decrease was not observed as the flow rate was increased in the new testing apparatus, indicating that the heater was in fact being cooled in the initial testing procedure.

Measuring the sensitivities of films with widely varying surface area:volume should have indicated a larger difference in slope values for the sensitivities. Figure 7 shows that the slope values are still close, indicating that other sources of error were occurring. These sources may have been variations in thermocouple and heater element contact with the diamond films, differences in thermal diffusivities or surface roughness of the films, and differences in hot wire placement with the flow. Average standard deviations were 0.7 and 0.6 for samples 3 and 7, respectively, indicating that systematic errors were still minimal.

Several suggestions are proposed as reasons for the inconclusive results. First, application of the epoxy could not be well controlled, and the amounts used from film to film differed. Thus, the contact area of the thermocouples and the heater element with the films differed. Improper contact could have resulted in insufficient sensing of temperature changes.

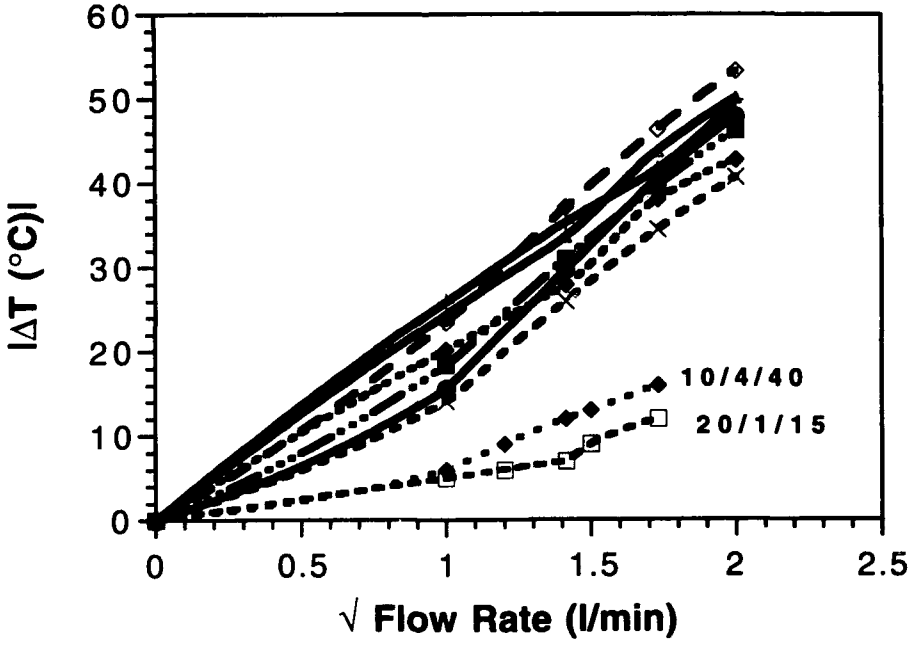

Figure 7. Sensitivities measured by the new testing procedure for two geometries. The new results are indicated on the same axes as the previous curves to show that better control of the heat supply to the film caused less of a drop in temperature. This comparison indicates that heater side cooling was occurring in the initial procedure.

Second, the thermal diffusivities may not have been the same in each film. Therefore, the speculated dependence of response time solely on surface area:volume may have been invalid.

Third, hot wire anemometer calibration is highly dependent upon position of the wire probe with the flow [11]. In order to accurately compare film geometries for sensitivity, they must be positioned in exactly the same manner.

Finally, variations in surface roughness of the diamond films could have played a role in response and sensitivity data. Though the topography of the 15μm and 40μm films appeared to be similar, each film was not observed individually. Thus, discrepancies between films used for actual calibration could have been present. Roughness seemingly has no effect on the hydrodynamic behavior of laminar flow. However, in turbulent flow the velocity distributions depend on the height of the rough projections and the heat conduction in the viscous sublayer which flows between the projections and separates the wall from the turbulent core of the stream.[10]

D. Summary

The objective of this project was to observe the effects of geometrical variations of diamond films on the response times and sensitivities of hot wire anemometer structures. Hot wire anemometer structures were designed using diamond as the thermal element. Changes in temperature as a function of flow rate were observed. Response times and sensitivities were measured for eight geometries that varied in length, width, and thickness. The structures showed poor agreement with King's law, and no correlations were shown between response times, sensitivities, and geometrical variations.

Inconclusive results were attributed to the observance of heater-side cooling of the structures. To test this hypothesis, a temperature controller was added to the system, and modifications were made in the gas line. Sensitivity was then determined for wires with a large variation in surface area:volume. The system upgrade did not significantly improve sensitivities, thus indicating that other sources of error may have been occurring.

E. Future Work

Several suggestions are proposed in order to properly test the geometrical effects on response times and sensitivities of the hot wire anemometer structures:

1) Diamond films should be used that have very similar topographies, and the topography of each film used in the actual calibration should be observed with a microanalysis technique (SEM). Utilizing films of similar topography and morphology should alleviate differences caused by varying surface roughness and thermal diffusivities.

2) The fabrication of the structures needs to be optimized to allow standardization from structure to structure, i.e., the amount of epoxy, the contact area with the support, and the wire placement should be uniform.
3) Structures should be designed with the heater element protected from the flow.
4) A digital power source with small increments in voltage and current (e.g. millivolts and amps) should be utilized to measure exact power inputs in the heat transfer calibration tests.
5) Finally, an accurate flow meter that has the ability to gage small flow rate increments should be employed.

The next step in diamond thin film hot wire anemometry research is developing a process flow for diamond films patterned on silicon substrates that can be completely back etched to leave the sensitive diamond area free standing. Wafer size, masking layer (SiO_2) thickness, exposure and development times, and masking material must be taken into consideration.

Finally, hot wire anemometers are very temperature-sensitive; this affects the measurement of the average flow velocity. Therefore, additional wires have been added for thermal compensation. The additional wire is a temperature sensor whose readings are used to correct the readings of the flow sensor. Thus far, the additional wires used cannot measure changes in temperature fast enough.[12] A diamond thermistor could be used as a temperature-compensator on a diamond hot wire anemometer. The thermistor would exhibit a rapid enough response to correct for the velocity sensor readings.

F. References

1. J. P. DeCarlo, *Fundamentals of Flow Measurement,* Mass: Foxboro Co., 1984.
2. L. V. King, Philos. Trans. of the Royal Soc. of London **214**, (1914) 373.
3. A. E. Perry, *Hot-Wire Anemometry,* New York: Oxford Univ. Press, (1982).
4. T. Roppel, C. Ellis, R. Ramesham, D. Jaworske, M. E. Baginski, and S. Y. Lee, *Applic. of Diamond Thin Films and Related Matls.*, 311 (1991).
5. T. Roppel, R. Ramesham, C. Ellis, and S. Y. Leel, Thin Solid Films **212**, 56 (1992).
6. P. J. Schneider, *Conduction Heat Transfer,* Mass: Addison-Wesley Publishing Co., Inc. (1955).
7. M. A. Swaminathan, G.W. Rankin, and K. Sridhar, J. of Fluids Engr. **108**, 115 (1986).
8. H. H. Bruun, M. A. Khan, H. H. Al-Kayiem, and A.A. Fardad, J. Phys. E: Sci. Instrum. **21**, 225 (1988).
9. C. J. Geankoplis, *Transport Processes and Unit Operations,* 3rd ed. New Jersey: Prentice Hall (1993).
10. S. Kutateladze, *Fundamentals of Heat Transfer,* NY: Academic Press, (1963).
11. G. Buresti and A. Talamelli, Meas. Sci. Technol. **3** 17, (1992).
12. A. V. Smol'yakov and V. M. Tkachenko, *The Measurement of Turbulent Fluctuations: An Introduction to Hot-Wire Anemometry and Related Transducers,* New York: Springer-Verlag, (1983).
13. J. E. Graebner, S. Jin, G. W. Kammlott, B. Bacon, and L. Seibles, J. Applied Physics **71**, 5353 (1992).
14. D. Lide, Ed., *CRC Handbook of Chemistry and Physics,* 73rd ed. Boca Raton, FL: CRC Press, 4-36, 12-78, 130 (1992-93).

III. Growth and Characterization of Cubic Boron Nitride Thin Films

A. Introduction

Boron nitride, like carbon, forms with three crystalline structures: a layered hexagonal form (h-BN) which is similar to graphite; cubic boron nitride (c-BN) which corresponds to diamond; and a rarer form, wurtzitic boron nitride (w-BN), which is analogous to Lonsdaleite. The last two phases are metastable at moderate temperatures and pressures.

The interest in c-BN films stems from their potential applications as hard coatings and from their electronic and thermal properties. Cubic BN is the hardest known material other than diamond. Unlike diamond, c-BN does not react with ferrous metals, and it can be used at higher temperatures before the onset of structural transformation. These properties ma' an excellent cutting tool material. Bulk c-BN crystals formed using high temperatu h pressure techniques are already used in the cutting tool industry. Electronic applications of cubic boron nitride would take advantage of its very wide band gap ($E_g \approx 6.4$ eV [1]), its ability to be doped both p-type and n-type with Be and Si, respectively [2], and for some applications its very high thermal conductivity.

Cubic boron nitride was first grown in bulk crystal form in 1956 [3]. Reports of c-BN in thin film form appeared as early as 1970 [4], but it was not until about 1987 that thin films conclusively characterized as cubic boron nitride were achieved [5]. Subsequently, many groups have successfully grown c-BN using various techniques including ion beam assisted deposition [6,7] r.f. sputtering [8], ion plating [9], laser ablation [10,11], ECR plasma [12], and chemical vapor deposition (CVD) [13].

Cracking and loss of adhesion of deposited c-BN films are frequently reported phenomena, which have been attributed to a high level of intrinsic compressive stress in the films [14,15]. Murakawa [9] has attempted to overcome this problem using buffer layers between the substrate and the BN film, including a graded B to BN layer and a TiN layer, together with post-deposition annealing of the films. Okamoto *et al.* [16] also used a graded B to BN buffer layer in CVD c-BN films. Both studies produced well adhered films. No reports have appeared of stress-free c-BN films grown directly on a substrate. By contrast, recent research strongly indicates that a high stress level in the film is a necessary condition for the formation of the cubic phase [15, 17].

An additional challenge is growing epitaxial films, which would be essential for the majority of electronic device applications. No reports of reproducible experiments of epitaxial growth of c-BN have appeared. A better understanding of what happens at the substrate-BN interface needs to be developed. In a previous paper [17] we have shown that when BN is deposited on Si, initial amorphous and hexagonal BN layers grow before cubic

growth begins. If these interfacial layers are necessary precursors to c-BN growth, then it would appear exceedingly challenging to grow epitaxial c-BN using current PVD methods.

An area of research where significant progress has been made is in determining the deposition conditions necessary for c-BN growth. The work of Kester and Messier [18] established that for a given substrate temperature, the momentum transferred into the growing film by the bombarding ions is the single parameter which controls the formation of c-BN. As long as sufficient N is present, a threshold value of momentum transfer exists for the formation of c-BN. This controlling parameter incorporates the values of ion energy, ion flux, and ion species. As a result of the present study described below we have developed a better understanding of both the conditions required for c-BN growth and of the mechanisms responsible for that growth.

B. Experiment

Deposition. Ion beam assisted deposition (IBAD) has been used successfully for c-BN growth [17,18]. It is particularly useful in that the B deposition rate, bombarding ion energy, ion flux and ion species can be controlled and measured independently. This allows for good quantification of the deposition process. The IBAD configuration in the present study employed electron beam evaporation of boron together with simultaneous bombardment by nitrogen and argon ions from a Kaufman ion source. A schematic of the deposition system is shown in Fig. 1.

The substrates used in this study were (100) single crystal infrared-transparent, high resistivity (ρ>50 Ω-cm) on-axis Si; cut and polished single crystal natural diamond; as well as polished single crystal Cu and Ni. The Si substrates were cleaned using a standard RCA procedure [19] of which the final step was a 5 min dip in 10% HF. This left the surface H terminated, as determined by XPS. The diamond substrates were etched in a boiling 3:4:1 H_2SO_4:HNO_3:$HClO_4$ solution for 45 minutes to remove any graphitic phase, and the Cu and Ni substrates were decreased ultrasonically in a sequence of TCE, acetone, methanol, and DI water. The substrates were attached to Mo holders using Ag paint which acted both as an adhesive and a thermal conductor. This assembly was subsequently loaded through a vacuum load lock into the UHV deposition chamber. Base pressures in the chamber were typically $5\text{-}8 \times 10^{-10}$ Torr.

Each substrate was heated using a W wire coil located behind the Mo substrate holder. They were baked under UHV conditions at 700°C for 20 min to remove residual H_2O and hydrocarbon species. The substrate temperature during deposition was monitored using thermocouples near the heater, the readings of which had been previously calibrated to several temperatures of the substrate surface. Boron was deposited using a constant deposition rate of 0.5 Å/s, which was monitored using a quartz crystal rate monitor. Fluxes of

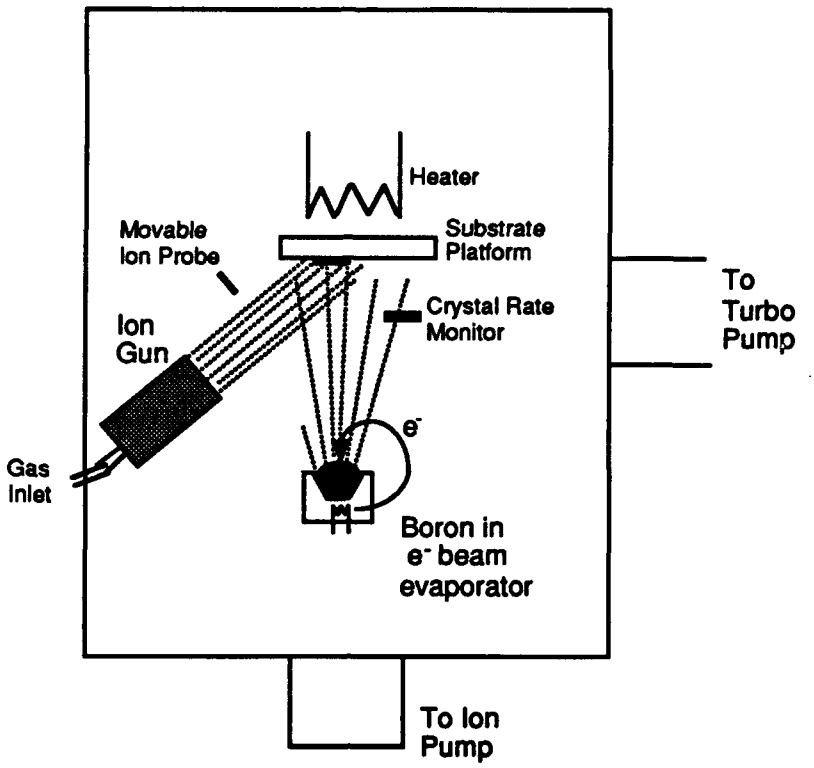

Figure 1. Schematic of UHV electron beam evaporator-based IBAD system used in this research.

N and Ar ions were obtained from a 3 cm Ion Tech Kaufman source. Argon and nitrogen gases were used with a gas flow ratio of 1:1. Because of the close ionization potentials of these two gases, the ion ratio was also close to 1:1. The ion source was operated at 500 eV; based on the studies of Hubler *et al.* [20] the N ions were predominantly N_2^+. The discharge voltage of this source was maintained at a sufficiently low value to prevent double ionization of either species. Since it has been previously shown that c-BN can be successfully deposited using an $Ar:N_2$ ratio of 1:1 and an ion energy of 500 eV [17,18], these values were maintained constant throughout this study.

Both the ion beam and the boron evaporation were started and allowed to stabilize before deposition. During this period, the substrate was covered by a movable shutter. To eliminate the potential for surface damage, there was no pre-deposition ion bombardment of the substrates.

Characterization methods. The primary method of film characterization was Fourier transform infrared spectroscopy (FTIR) due to the ability to distinguish between the cubic and hexagonal or amorphous forms of BN. Cubic BN has a transverse optical mode absorption peak at 1075 cm^{-1}, while amorphous and hexagonal BN have a primary absorption peak at 1367 cm^{-1} and a secondary peak at 783 cm^{-1} [21,22]. The spectra were obtained using an Analect Instruments model fx-6260 spectrometer. The IR beam was passed through the

BN coated substrate. A ratio of the resultant spectrum to that obtained from a background scan taken from an uncoated substrate was determined. Reflectance FTIR was employed to characterize the films deposited on the IR opaque Cu and Ni substrates. The latter study was conducted on a Nicolet 620 FTIR equipped with a Spectra Tech IR Plan optical microscope.

The film crystallography and the film-substrate interface were studied via high resolution cross sectional transmission electron microscopy (HRTEM) using a JEOL 4000EX operated at 400kV. The images were recorded using a 1mr convergence semi-angle at a Scherzer defocus of ~ 47nm. Samples were prepared using standard techniques [23].

Rutherford backscattering spectrometry (RBS) was used to measure the compositions and thicknesses of the films due to this techniques ability to give a depth profile of the film, not only information about the surface layer. 2.0 MeV primary He^+ ions and a 165° scattering angle were used for measuring the energy of the backscattered nuclei. The samples were tilted 6° to prevent channeling.

C. Results

FTIR Results. The results reported in this and the following subsection were obtained using only Si(100) substrates. To study the effect of substrate temperature (T_S) on the BN films, depositions were conducted from 200°C to 700°C. All other variables were held constant. The results of one of these series of depositions are shown in Fig. 2. There was almost no cubic phase in the 200°C film. In the temperature range of 300-400°C, the films were a mixture of the cubic and hexagonal/amorphous phases (IR does not distinguish between the hexagonal and amorphous forms of BN). The relative amount of cubic phase increased with increasing temperature. At some temperature above 400°C the amount of cubic phase began to drop rapidly; it was not observed at all in the film deposited at 700°C. These results correspond well with those of other researchers [24] who have also found that the best temperature for growing cubic boron nitride is at or close to 400°C.

A second significant parameter studied was the ion bombardment flux. As discussed above, it has been previously shown [18] that the critical parameter (at constant temperature) for growing the cubic phase is momentum, p, transferred from the bombarding ions into the growing film per deposited boron atom, p/a, where a is the boron flux measured in atoms $cm^{-2}\ s^{-1}$. This critical value is given by

$$\frac{p}{a} = \frac{J}{a}\sqrt{2m\gamma E} \qquad (1)$$

where J/a is the ratio of bombarding ions to depositing boron atoms. J is the ion flux measured in ions $cm^{-2}\ s^{-1}$, m is the mass of the bombarding ions and E is their energy. The maximum energy transfer from the ion to the atom, γ, is given by

$$\gamma = \frac{4mM}{(m+M)^2} \tag{2}$$

with M being equal to the average mass of the atoms being bombarded. There is a linear relationship between the ion flux, J, and the momentum transfer value. Therefore a change in the ion flux (while keeping the ion energy and ion species distribution constant) acts directly as a change in momentum transfer. Since changing the ion energy, E, has less of an effect on the momentum (momentum being proportional to the square root of the energy), the bombardment level in this study was varied by varying the ion flux and keeping the ion energy constant.

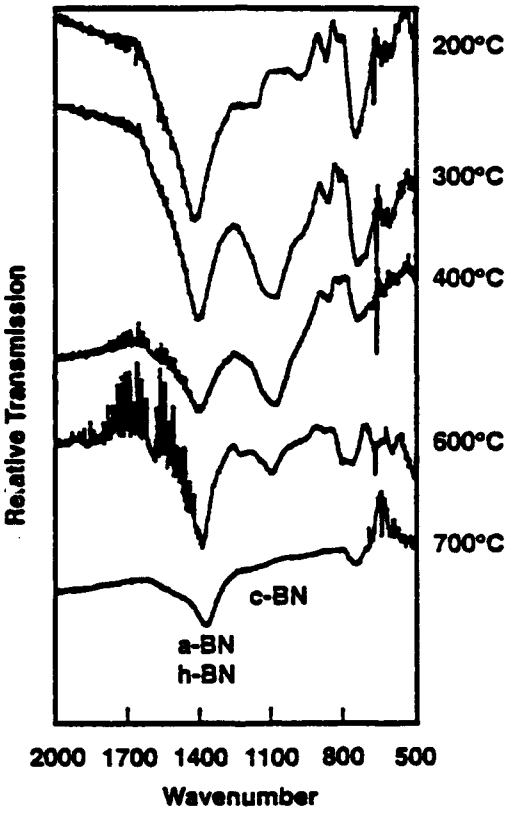

Figure 2. FTIR spectra of BN films deposited on Si(100) at various substrate temperatures. Other deposition conditions were film thickness: 200Å; ion flux: 0.32 mA/cm^2; boron deposition rate: 0.5 Å/s; ion energy: 500 eV; ion bombardment by 50:50 Ar:N_2.

Fig. 3(a) shows the effect of changing the ion flux while keeping the temperature constant at 600°C. Essentially no cubic phase is observed until the ion flux reaches 0.30 mA/cm^2. The small peaks observed at 1050–1100 cm-1 at the two lower flux values are due to the Si substrate. This confirms that there is a minimum momentum transfer level, and therefore ion flux, necessary to grow the cubic phase at a given temperature. The spectra shown in

Fig. 3(b) are from films grown at the same conditions as those in Fig. 3(a), except at 400°C. There is a small cubic peak visible at 0.20 mA/cm^2, and the films are predominantly cubic at 0.24 and 0.30 mA/cm^2. Comparing Figs. 3(a) and (b) confirms the result seen in Fig. 2 that increasing the substrate temperature above 400°C lowers the proportion of cubic phase in the film.

The data presented above indicated that increasing the ion flux, and thereby the momentum transfer, increases the amount of cubic phase in a film, and that increasing the substrate temperature above 400°C decreases the proportion of cubic phase. However, our previous FTIR and HRTEM results [17] showed that the relative amount of each phase in a 400°C film was also a function of film thickness. These films contained very thin amorphous and hexagonal layers of essentially constant thickness prior to the nucleation and growth of the c-BN layer. Nucleation of the pure cubic phase did not occur until a specific total thickness of the non-cubic phases was achieved.

As such, the FTIR spectra of films of different thicknesses deposited under identical conditions showed that the thicker films had a higher cubic to non-cubic ratio. Examination of films of different thicknesses prepared using the conditions of the 200Å thick 700°C film of Fig. 2, showed the same effect, as demonstrated in Fig. 4. The 100Å film and the 200Å films were completely amorphous/hexagonal, but the 400Å film was predominantly cubic. Similarly, FTIR of a set of films of different thicknesses prepared under the same conditions as the 600°C film of Fig. 2, revealed a growth sequence and layer thicknesses of non-cubic (<200Å), partially cubic (200Å), and predominantly cubic (remainder of film). These results indicate (and the HRTEM results noted below prove) that the different proportions of amorphous/hexagonal and cubic phase found in the different films are not due to different amounts of each phase interspersed through the film, but rather to the transition from single phase hexagonal to single phase cubic occurring at varying thicknesses depending on growth conditions. Specifically, the differences between the 400°C, 600°C, and 700°C films seen in Fig. 2, which ranged from significantly cubic at 400°C to completely non-cubic at 700°C are due to varying thicknesses at which the growth of the cubic phase layer begins. A higher substrate temperature delays the onset of the cubic phase. Increased ion flux enhances the onset of this phase.

HRTEM results. High resolution TEM images of films deposited at 200°C, 400°C, and 700°C are shown in Figures 5(a), 5(b), and 5(c). The film deposited at 200°C (Fig. 5(a)) has a 70Å amorphous layer at the Si interface followed by a layer of oriented h-BN. No c-BN is present. The film deposited at 400°C (Fig. 5(b)) has a 20Å amorphous layer followed by 50Å of oriented h-BN followed by c-BN. The film grown at 700°C (Fig. 5(c)) has a 50Å amorphous layer followed by a ~150Å layer of predominantly partially oriented h-BN material with a small amount of c-BN, followed by a c-BN layer.

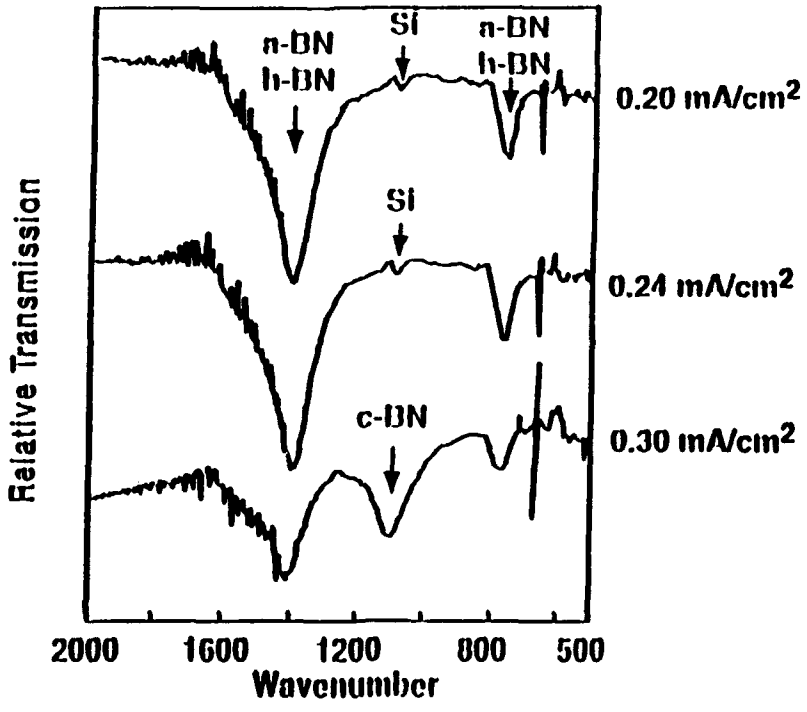

Figure 3 (a). FTIR spectra of a BN film deposited on Si(100) with various ion bombardment fluxes at a substrate temperatures of 600°C. Other deposition conditions were film thickness: 250Å; boron deposition rate: 0.5 Å/s; ion energy: 500 eV; ion bombardment by 50:50 Ar:N_2.

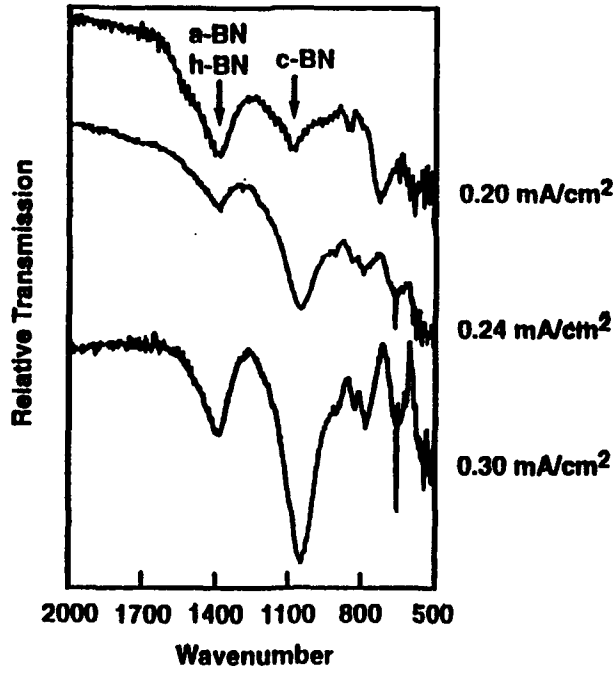

Figure 3 (b). FTIR spectra of a BN film deposited on Si(100) with various ion bombardment fluxes at a substrate temperatures of 400°C. Other deposition conditions were film thickness: 250Å; boron deposition rate: 0.5 Å/s; ion energy: 500 eV; ion bombardment by 50:50 Ar:N_2.

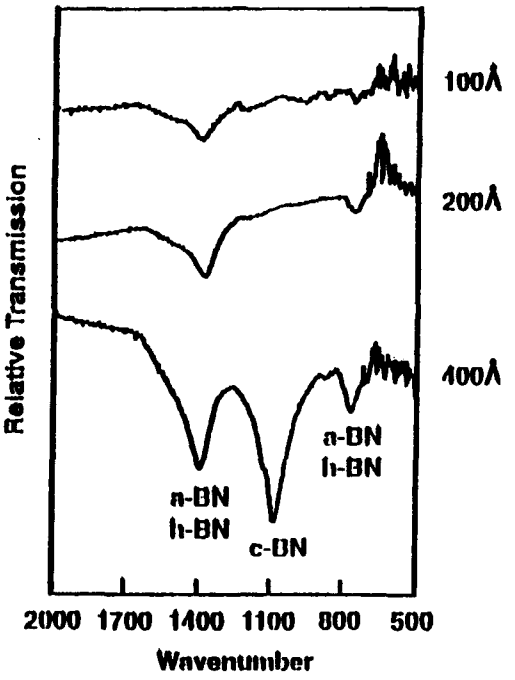

Figure 4. FTIR spectra of BN films deposited on Si(100) with various thicknesses. Other deposition conditions were substrate temperature: 700°C; ion flux: 0.32 mA/cm^2; boron deposition rate: 0.5 Å/s; ion energy: 500 eV; ion bombardment by 50:50 Ar:N_2.

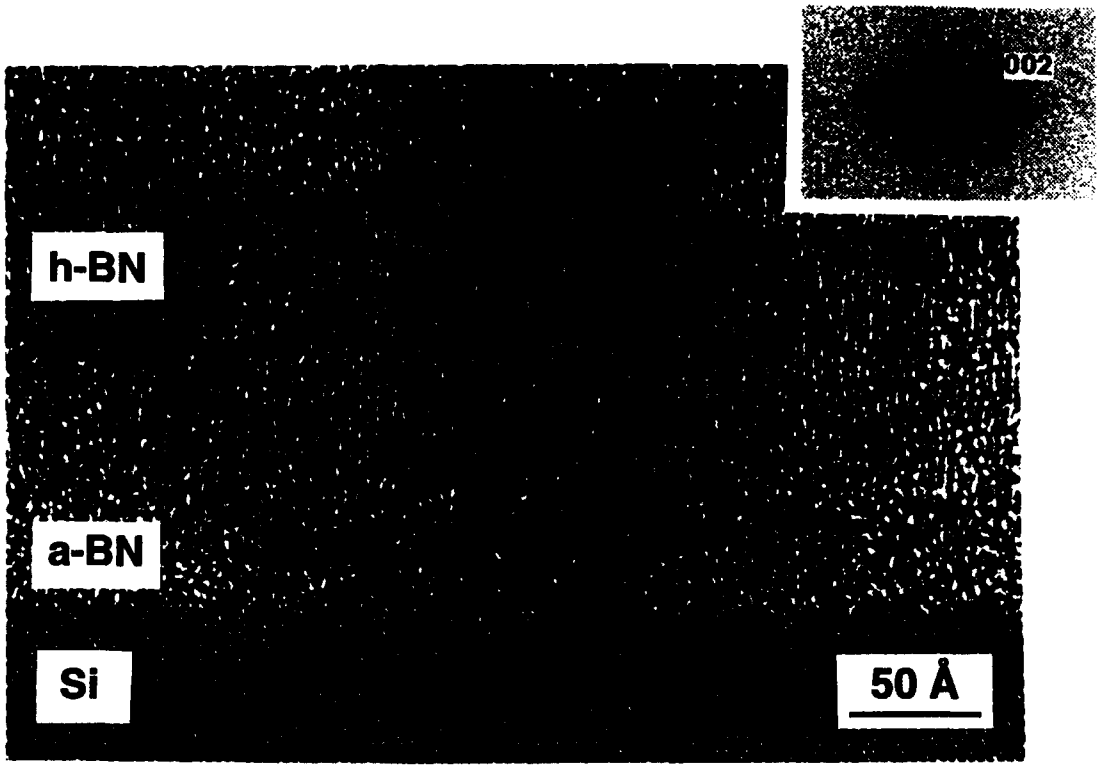

Figure 5(a). HRTEM image of a film deposited on Si(100) at 200°C. Other deposition conditions were ion flux: 0.28 mA/cm^2; boron deposition rate: 0.5 Å/s; ion energy: 500 eV; ion bombardment by 50: 50 Ar:N_2.

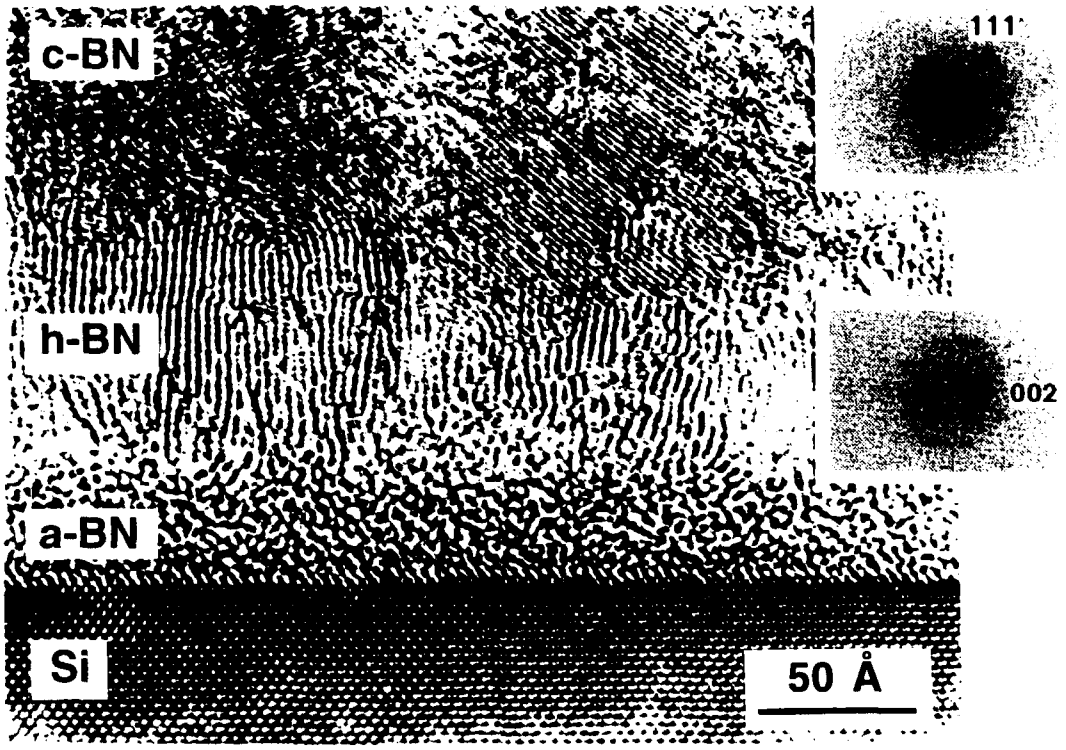

Figure 5(b). HRTEM image of a film deposited on Si(100) at 400°C. Other deposition conditions were ion flux: 0.12 mA/cm^2; boron deposition rate: 0.25 Å/s; ion energy: 500 eV; ion bombardment by 50: 50 Ar:N_2.

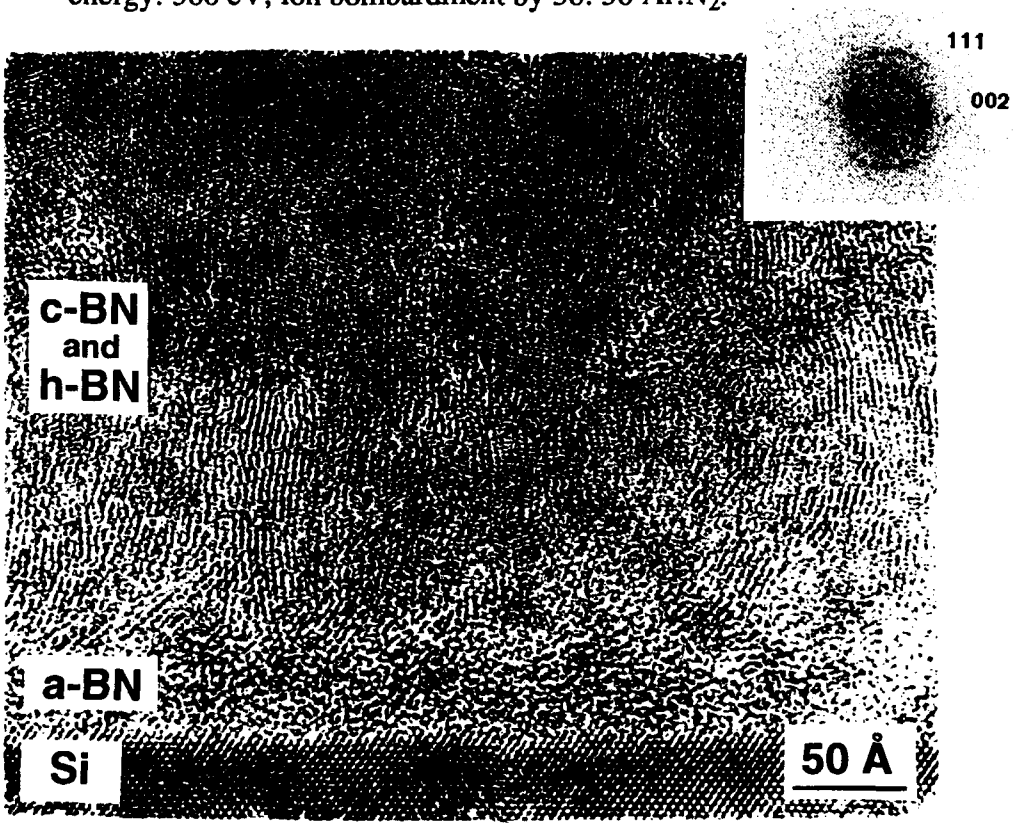

Figure 5(c). HRTEM image of a film deposited on Si(100) at 700°C. Other deposition conditions were ion flux: 0.28 mA/cm^2; boron deposition rate: 0.5 Å/s; ion energy: 500 eV; ion bombardment by 50: 50 Ar:N_2.

RBS Results. The BN grown for RBS was deposited on the lower atomic number substrate of Be to circumvent overlap of the spectra of the Si substrate with that of the film. The deposition conditions were those which resulted in c-BN growth on Si: a substrate temperature of 400°C, ion energy of 500eV, and an ion flux of 0.24 mA/cm^2. The film thickness was 500Å. The results are shown in Fig. 6. Rutherford backscattering is more sensitive to elements of higher atomic number, due to their larger nuclear cross sections. Therefore, the sizes of the original peaks at various channel numbers do not directly show their actual concentration. Computer modeling of the spectra revealed that in addition to the expected Be, B, and N, there was O due to a BeO layer on the substrate as well as Ar, Fe, and Hf in the film having the atomic percentages of ~1.5%, ~0.2%, and ~0.05%, respectively. The Ar was derived from the ion bombardment during growth; the Fe was probably due to the ion beam bombardment of the stainless steel shutter above the substrates, and the Hf was very likely derived from resputtering of residual amounts previously deposited on the substrate block.

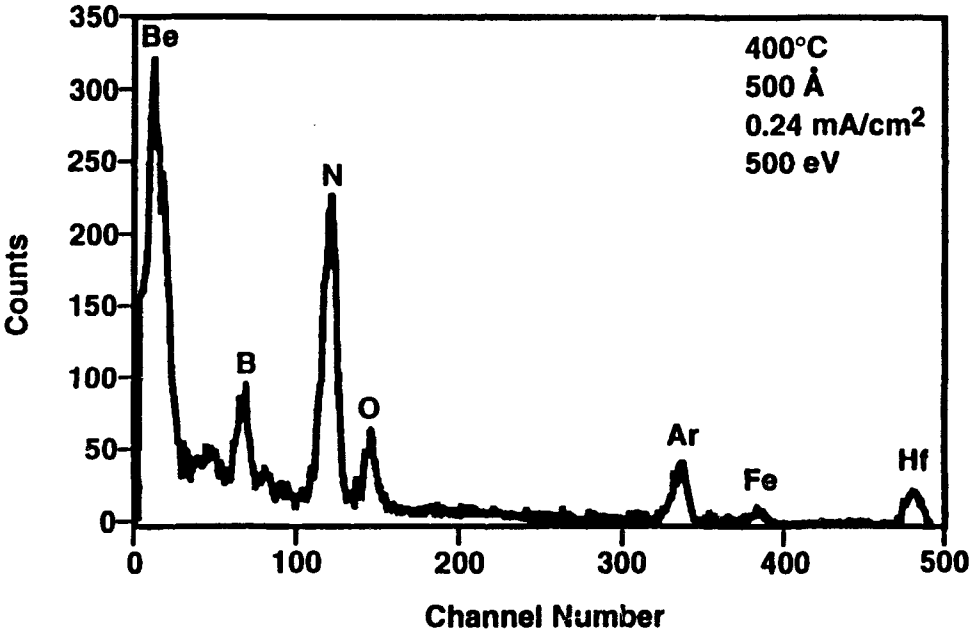

Figure 6. RBS spectra of a BN film on a beryllium substrate. Deposition conditions were film thickness: 500Å, substrate temperature: 400°C; ion flux: 0.24 mA/cm^2; boron deposition rate: 0.5 Å/s; ion energy: 500 eV; ion bombardment by 50:50 Ar:N_2.

Other Substrates. Films having a thickness of 1000 Å were grown on diamond at substrate temperatures of 400° and 600°C using an ion energy of 500eV and an ion flux of 0.24 mA/cm^2. A representative FTIR pattern of one of the films deposited at 400°C is shown in Fig. 7. A sharp c-BN peak is observed at ~1080 cm^{-1}. The h-BN peak is very small. The

spectrum of this relatively thick film has a sharper c-BN peak and a better c-BN to h-BN ratio than any of the films we had previously deposited on Si, and is as good or better than any that have previously appeared in the literature. For the film grown at 600°C the FTIR spectrum was essentially the same.

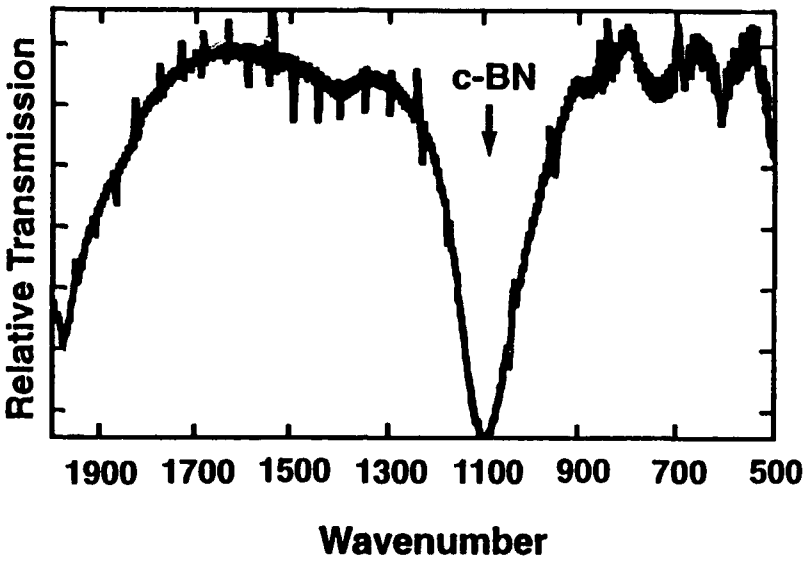

Figure 7. FTIR spectra of BN deposited on a single crystal diamond(100) substrate. Deposition conditions were film thickness: 1000Å, substrate temperature: 400°C; ion flux: 0.24 mA/cm^2; boron deposition rate: 0.5 Å/s; ion energy: 500 eV; ion bombardment by 50:50 Ar:N_2.

Observation via SEM of the films deposited at 400°C showed occasional cracking. The films deposited at 600°C showed no cracking or delamination. Films deposited under the same deposition conditions and the same thicknesses on Si exhibited both severe cracking and delamination.

High resolution TEM was performed on the sample grown at 600°C, and an image is shown in Fig. 8. The same type of layered structure observed on BN grown on Si is present, although not as pronounced.

Nickel and Cu also have lattice spacings very close to that of c-BN, with a lattice mismatch for Ni of 2.6% and for Cu of less than 0.05%. Therefore it was thought that like diamond (which has a lattice mismatch of 1.4%) they may be better substrates for c-BN growth than Si which has a lattice mismatch of 33%. Films having a thickness of 500Å were grown at 400°C under the same conditions of ion flux and ion energy employed in the deposition on diamond. As shown in Fig. 9, reflectance FTIR from films grown on the Ni

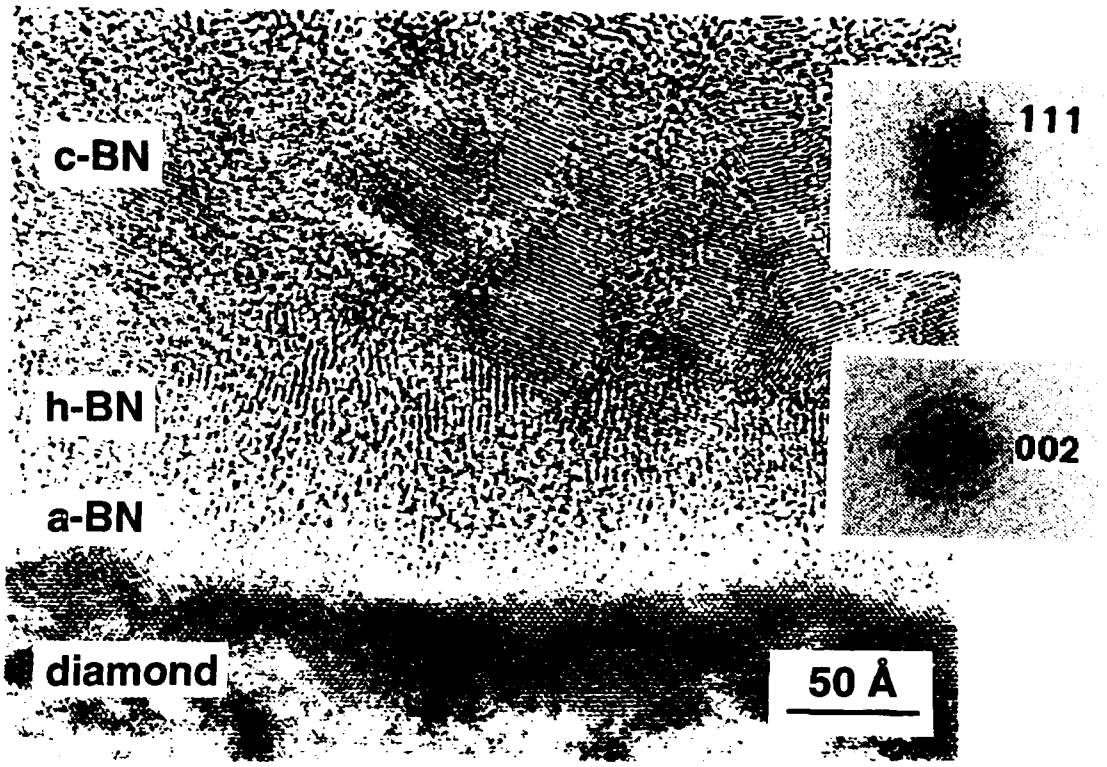

Figure 8. HRTEM image of a 600°C film on a diamond(100) substrate. Other deposition conditions were ion flux: 0.28 mA/cm^2; boron deposition rate: 0.5 Å/s; ion energy: 500 eV; ion bombardment by 50:50 Ar:N_2.

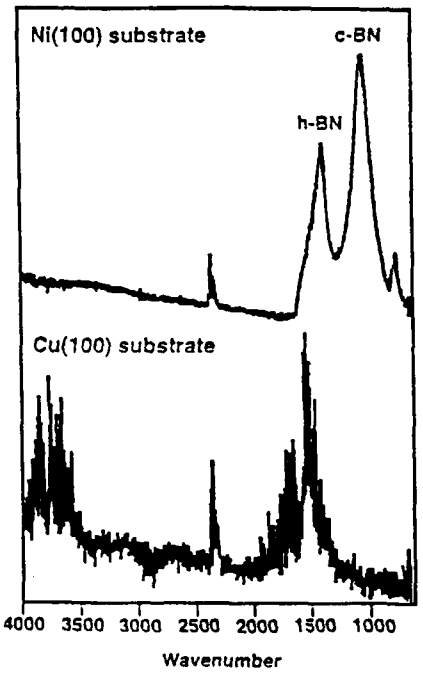

Figure 9. Reflectance FTIR of BN deposited on Cu(100) and Ni(100) substrates. Deposition conditions were film thickness: 500Å, substrate temperature: 400°C; ion flux: 0.24 mA/cm^2; boron deposition rate: 0.5 Å/s; ion energy: 500 eV; ion bombardment by 50:50 Ar:N_2.

substrate revealed a mixture of h-BN and c-BN; films grown on Cu were h-BN with no evidence of c-BN.

D. Discussion

The above results show that the onset of c-BN growth is a function of temperature, ion momentum transfer and deposition period (film thickness). McKenzie *et al.* [14,15] have shown theoretically and experimentally that the effect of deposition period is caused by the build-up of biaxial compressive stresses in the growing film. They observed by FTIR, electron energy loss spectroscopy and TEM an initial layer of h-BN oriented perpendicular to the substrate surface. The nucleation and growth of c-BN occurred as the stress in the film increased. No amorphous phase was reported. The stress at the onset of c-BN growth corresponded to conditions in the high pressure regime where this phase is stable. The present results can be understood using this model. Increasing the substrate temperature from, for example, 400°C to 700°C, results in both a higher surface mobility of the adsorbed species and possibly bulk annealing, which allow stress relaxation. Thus, as shown in Fig. 4, the higher the deposition temperature the greater the film thickness necessary to reach the stress level required for c-BN nucleation and growth, all other conditions being the same. There is a sharp increase in the transition thickness, and therefore a sharp drop in stress, within the 600-700°C temperature range. This corresponds with the results of Windischmann [25] who found in several different materials, that increasing the deposition temperature from room temperature causes a gradual decrease in the intrinsic stress , followed by a sharp drop when the temperature reaches $T_m/3$, where T_m is the melting point. For BN, $T_m/3$ is ~700°C.

The foregoing explanation does not account for the results of decreasing the temperature below 400°C, for it does not further lower the threshold thickness for initiation of the cubic phase. In fact, at these lower temperatures, growth of the cubic material as a single phase was not observed. The existence of an apparent minimum in substrate temperature for the growth of pure c-BN indicates that the combination of thermal energy and intrinsic stress is insufficient for all the B and N atoms to surmount the activation energy barrier between the layered h-BN and the three-dimensional c-BN structure.

Similarly, an increase in ion flux and momentum transfer into the growing film will lead to a more rapid increase in stress, as shown by Kester and Messier [18] as well as Windischmann [25] and a decrease in the film thickness necessary for the initiation of the cubic phase. The results presented in Figs. 3(a) and (b) snow the onset of c-BN to be also a function of ion flux. These correspondences between known effects on stress and the onset of c-BN growth are strong evidence that the cubic phase growth results directly from stress.

The mechanism(s) which cause(s) the increase in stress in the films is not completely understood. It may be densification due to ion bombardment, as reported by [27]. The

densification occurs through the collapse of the void structure found in non-bombarded films. Nir [28] and Targove and Macleod [29] have shown experimentally that the magnitude of the compressive stress is a function of the momentum transfer to the growing surface for particle energies <1kV. Theoretical studies by Windischmann [30] support these findings. A second possibility is that the stress is due to the presence of interstitials in the film. In the case of the c-BN films, the relatively high concentration of Ar (1.5 at.%) as shown by RBS would suggest that the compressive stress may be caused by interstitial Ar atoms in the manner observed by McKenzie *et al.* [14].

In the growth of BN films via IBAD by Stambouli et. al. [31] using bombardment with nitrogen ions, it was found that sufficient bombardment by nitrogen ions resulted in nitrogen-rich (non-cubic) BN_{1+x} films with a higher density than stoichiometric BN films. The former also possessed significantly higher compressive stresses than the stoichiometric films. They attributed this to interstitial N. If this is the case, bombardment by the larger Ar ion, and the formation of interstitial Ar at 1.5 at.%, would be expected to also increase the compressive stress in the films. In fact, Fahnline *et al.* [32] showed that 1.5 at.% Ar in Ge films caused a significant increase in compressive intrinsic stress.

Kester and Messier [18] previously showed that the phase of BN films is determined by three factors: substrate temperature, bombardment measured in terms of momentum transfer, and stoichiometry. The stoichiometry factor was a requirement in that at least one bombarding N atom had to be present for each depositing B atom. They plotted the observed phase(s) as a function of temperature and bombardment. In the present study we have shown that these are controlling parameters, but they control not only whether or not cubic growth will occur, but the time of nucleation and growth of this phase. Some of the conditions that they described as leading to mixed cubic and hexagonal growth appear to be conditions leading to layered single phase hexagonal followed by single phase cubic growth.

The problem of adhesion of c-BN on Si was addressed by using substrates with better lattice matching to c-BN including Cu and Ni and diamond. The cubic phase did not grow on the Cu(100) substrate due to its excellent ductility which adsorbed the stresses generated in the growing film; it did grow on the less ductile Ni(100) substrate, but the adhesion was as poor as on Si. These results indicate that the adhesion problem is not simply one of lattice mismatch with the substrate.

Adhesion on the diamond substrates was much better than on the other materials. Although a relatively small number of samples were produced, due to the prohibitive cost, these results suggest that c-BN does not easily grow initially on diamond even though this substrate has a higher surface energy than c-BN. Moreover, these results imply that c-BN will not initially deposit on any material, at least by the methods used in this investigation.

E. Conclusions

Boron nitride films deposited using ion beam assisted deposition on Si, diamond and Ni substrates grow in a sequence of amorphous, hexagonal and cubic layers. This is believed to be caused primarily by the increased incorporation of intrinsic biaxial compressive stresses in the films. The nucleation of the cubic phase occurs at differing film thicknesses as a function of both substrate temperature and ion flux. There appears to be a minimum substrate temperature (200–300°C) below which single phase growth of c-BN does not occur. At higher temperatures the onset of the cubic phase is a function of temperature, appearing at greater thicknesses at higher temperatures under the same ion flux. This is attributed to increased adatom mobility and bulk annealing with increasing temperature and a concomitant relaxation of stress. For these reasons the optimum temperature range for the growth of c-BN was determined to be 400-500°C. This range in T is similar to that determined by other investigators. Increased ion bombardment, as measured by momentum transferred into the film, leads to an earlier start of cubic growth, apparently due to the increased stress. It is suggested that the stress in the films may be due to Ar interstitials. The fact that stress is a function of momentum transferred into the film may be due to higher momentum bombardment (higher flux, energy or ion mass) leading to deeper and/or a greater number of interstitials.

We were unable to nucleate c-BN as the initial phase on any substrate; we suspect that this may prove difficult using bombardment based deposition methods due to the requirement of increasing stress generation in the films.

E. Acknowledgements

The authors express their appreciation to the Electronic Materials Center of Kobe Steel, USA and the Strategic Defense Initiative via the Office of Naval Research (Contract No. N00014-92-J-1720) for support of this research, to Dr. Nalin Parikh of the University of North Carolina-Chapel Hill for the RBS measurements, to Professor D. R. McKenzie of the University of Sydney and Lisa M. Porter, R. C. Glass and M. J. Paisley of NCSU for helpful discussion.

F. References

1. L. Vel, G. Demazeau, and J. Etourneau, Materials Science and Engineering **B10**, 149 (1991).
2. K. Era, O. Mishima, Y. Wada, J. Tanaka, and S. Yamaoka, in Electroluminescence, edited by S. Shionoya and H. Kobayashi, Springer Proceedings in Physics, **38**, 386 (1989).
3. R. H. Wentorf, Jr., J. Chem. Phys. **26**, 956 (1957).
4. V. N. Gashtold *et al.*, Elektronnaya Tekhnika **12**, 58 (1970).
5. K. Inagawa, K. Watanabe, H. Ohsone, K. Saitoh, and A. Itoh, J. Vac. Sci. Technol. **A5**, 2696 (1987).

6. D. J. Kester and R. Messier, Mater. Res. Soc. Symp. Proc. **235**, 721 (1992).
7. T. Wada and N. Yamashita, J. Vac. Soc. Technol. **A10**, 515 (1992).
8. K. Bewilogua, J. Buth, H. Hübsch, and M. Grischke, Diamond and Related Materials **2**, 1206 (1993).
9. M. Murakawa, S. Watanabe, and S. Miyake, Diamond Films and Technol. **1**, 55 (1991).
10. G. L. Doll, J. A. Sell, C. A. Taylor II, and R. Clarke, Phys. Rev. B **43**, 6816 (1991).
11. T. A. Friedmann, K. F. McCarty, and E. J. Klaus, Applied Physics Letters **61**, 2406 (1992).
12. Y. Osaka, M. Okamoto, and Y. Utsumi, Mater. Res. Soc. Symp. Proc. **223**, 81 (1991).
13. H. Saitoh and W. Yarborough, Applied Physics Letters **58**, 2228 (1991).
14. D. R. McKenzie, W. D. McFall, W. G. Sainty, C. A. Davis and R. E. Collins, Diamond Relat. Mater. **2**, 970 (1993)
15. D. R. McKenzie, J. Vac. Sci. Technol. **A11**, 2758 (1993).
16. M. Okamoto, H. Yokoyama, and Y. Osaka, Japanese Journal of Applied Physics **29**, 930 (1990).
17. D. J. Kester, K. S. Ailey, R. F. Davis, and K. L. More, J. Mater. Res. **8**, 1213 (1993).
18. D. J. Kester and R. Messier, J. Appl. Phys. **72**, 504 (1992).
19. W. Kern and D. A. Puo-tinen, RCA Rev. **31**, 187 (1970).
20. D. Van Vechten, G. K. Hubler, and E. P. Donovan, Vacuum **36**, 841 (1986).
21. R. Geick and C. H. Perry, Phys. Rev. **146**, 543 (1966).
22. P. J. Gielisse, S. S. Mitra, J. N. Plendl, R. D. Griffis, L. C. Mansur, R. Marshall, and E. A. Pascoe, Phys. Rev. **155**, 1039 (1967).
23. C. H. Carter, Jr., J. A. Edmond, J. W. Palmour, J. Ryu, H. J. Kim and R. F. Davis in *Microscopic Identification of Electronic Defects in Semiconductors,* edited by N. M. Johnson, S. G. Bishop, and G. Watkins (Mater. Res. Soc. Proc., 46, Pittsburgh, PA 1985) pp. 593 -598.
24. N. Tanabe, T. Hayashi, and M. Iwaki, Diamond and Related Materials **1**,151 (1992).
25. H. Windischmann, J. Vac. Sci. Technol. **A7**, 2247 (1989).
26. H. Windischmann, J. Appl. Phys. **62**, 1800 (1987).
27. R. A. Roy and D. S. Yee, in *Handbook of Ion Beam Processing Technology*, edited by J. J. Cuomo, S. M. Rossnagel, and H. R. Kaufman, (Noyes, Park Ridge, NJ, 1989).
28. D. Nir, J. Vac. Sci. Technol. **A4**, 2954 (1986).
29. J. D. Targove and H. A. Macleod, App. Optics **27**, 3779 (1991).
30. H. Windischmann, J. Vac. Sci. Technol. **A9**, 2431 (1991).
31. V. Stambouli, O. Burat, D. Bouchier, and G. Gautherin, Surface and Coatings Technology **43/44**, 137 (1990).
32. D. Fahnline, B. Yang, K. Vedam, R. Messier, and L. Pilione, Mater. Res. Soc. Symp. Proc. **130**, 355 (1989).

IV. Distribution List

Mr. Max Yoder
Office of Naval Research
Electronics Program–Code 314
Ballston Tower One
800 North Quincy Street
Arlington, VA 22217-5660

Office of Naval Research
Resident Representative
The Ohio State Univ. Research Center
1960 Kenny Road
Columbus, OH 43210-1063

Director
Naval Research Laboratory
Attention: Code 2627
Washington, DC 20314

Defense Technical Information Center
Building 5
Cameron Station
Alexandria, VA 22314

Dr. Robert J. Markunas
Research Triangle Institute
Post Office Box 12194
Research Triangle Park, NC 27709-2194

Dr. Ron Rudder
Research Triangle Institute
P. O. Box 12194
Research Triangle Park, NC 27709-2194

Dr. Howard K. Schmidt
SI Diamond Technology, Inc.
2345 North Boulevard
Houston, TX 77098

Prof. Karl Spear
Pennsylvania State University
201 Steidle
University Park, PA 16802

Dr. Michael W. Geis
Lincoln Laboratories
244 Wood Street
P. O. Box 73
Lexington, MA 02173

Prof. R. F. Davis
Materials Science and Engineering
Box 7907
North Carolina State University
Raleigh, NC 27695-7907

Prof. R. J. Nemanich
Department of Physics
Box 8202
North Carolina State University
Raleigh, NC 27695-8202

Prof. John C. Angus
Chemical Engineering
Case Western Reserve University
Cleveland, OH 44106

Prof. Andrzej Badzian
271 Materials Research Laboratory
The Pennslyvania State University
University Park, PA 16802

Dr. H. Liu
Emcore Corp.
35 Elizabeth Avenue
Somerset, NJ 08873

Prof. Karen Gleason
Chemical Engineering, Rm. 66-462
M. I. T.
Cambridge, MA 02134

Prof. Jerry Whitten
Chemistry
Box 8201
N. C. State University
Raleigh, NC 27695-8201

Dr. Ray Thomas
Research Triangle Institute
Box 12194
Research Triangle Park, NC 27709-2194

Dr. Allen R. Kirkpatrick
Epion Corp.
4R Alfred Circle
Bedford, MA 01730

Dr. Robert C. Linares
Linares Management Assoc., Inc.
P. O. Box 336
Sherborn, MA 01770

Dr. Martin Kordesch
Physics
Clippinger Research Laboratories
Ohio University
Athens, OH 45701-2979

Prof. Charter Stinespring
Chemical Engineering, Box 6101
West Virginia University
Morgantown, WV 26506

Prof. Robert Hauge
Chemistry
Rice University
Houston, TX 77251

Dr. John Margrave
HARC
4800 Research Forest Drive
The Woodlands, TX 77381

Dr. John Posthill
Research Triangle Institute
P. O. Box 12194
Research Triangle Park, NC 27709-2194

Dr. James Butler
NRL Code 6174
Washington, DC 20375

Dr. Andrew Freedman
Aerodyne Research, Inc.
45 Manning Road
Billerica, MA 01821

Prof. Michael Frenklach
Penn State University
202 Academic Projects Bldg.
University Park, PA 16802

Prof. Jeffrey T. Glass
Materials Science & Engr.
Box 7907
North Carolina State University
Raleigh, NC 27695-7907

Dr. Warren Pickett
Code 6604
Naval Research Laboratory
Washington, DC 20375-5345

Prof. Max Swanson
Physics
University of North Carolina
Chapel Hill, NC 27599-3255

Dr. James Zeidler
Code 7601
NRaD
San Diego, CA 92152